journal

Processing of Hierarchical and Anisotropic Porosity LSM-YSZ Composites

Aaron Z. Lichtner,[‡,*] David Jauffrès,[§] Christophe L. Martin,[§] and Rajendra K. Bordia[‡,**,†]

[‡]Department of Materials Science and Engineering, University of Washington, Seattle 98195, Washington

[§]SIMaP Laboratory, Université de Grenoble, CNRS, BP 46, Saint Martin d'Hères Cedex 38402, France

Aqueous dispersions of lanthanum strontium manganite (LSM) and yttria-stabilized zirconia (YSZ) particles were controllably freeze-cast and then partially sintered resulting in anisotropic, hierarchically porous ceramics for Solid Oxide Fuel Cell (SOFC) cathodes. The resulting microstructures have aligned pores with a characteristic spacing (λ) between pore centers. The effect of freezing rate, slurry viscosity, and solid loading on solidification velocity and resultant microstructures was explored. Varying these parameters resulted in samples with a range of independently controllable and reproducible microstructures. Homogenous dispersion of LSM and YSZ in the freeze-cast structures was confirmed through elemental mapping. Freezing rate was found to have a significant effect on λ while solid loading affected overall porosity and ceramic wall-to-pore size ratio but had only a small influence on λ. Viscosity was found to have a complex albeit small impact on λ but a significant effect on particle dispersion and colloid stability.

I. Introduction

CONVENTIONALLY made SOFC electrodes suffer from a lack of microstructural control at different length scales.[1–3] Typically, a paste or powder mixture which may contain fugitive pore formers is applied and then sintered to an electrolyte through a screen-printing or tape-casting procedure.[2,4,5] The isotropic microstructures which result tend to have highly tortuous gas and percolation pathways which hinder gas flow and lead to reduced efficiencies.[5] In addition, the resulting structure, though highly porous, has isotropic mechanical and thermal properties which are nonideal for the anisotropic stresses experienced during the cell's lifetime.[1,3,5] Future improvements to SOFC technology will require higher degrees of both designed porosity and strength, and these two seemingly contradictory properties may be resolved by creating an engineered ceramic with an anisotropic and/or hierarchical microstructure.[5–7]

Using an anisotropic microstructure, an electrode could be designed to efficiently guide gas flow along short, direct pathways to the triple phase boundaries (TPBs) where electrochemical reactions take place, thus improving conversion efficiency. In addition, anisotropic microstructures can provide direct percolation pathways for ionic and electronic species within the cathode, electrolyte, and current collectors which would be a significant improvement over conventional SOFCs.[3,5,8,9] Anisotropic structures could be designed to provide increased strength in the direction of mechanical loading, i.e., in-plane of the cell. Therefore, an optimally tailored anisotropic and hierarchical microstructure should allow for optimization of pore sizes; improved gas flow, maximization of the TPBs, increased strength, and an overall increase in cell lifetime.[4,5,8–10]

Freeze-casting is a technique that exploits the highly anisotropic solidification behavior of a solvent (generally water) in a well-dispersed slurry to controllably template a directionally porous ceramic.[6,7] During the freezing process, ice crystals grow, pushing ceramic particles from the liquid phase aside so that they accumulate between the growing ice crystals, the resultant microstructures from this process contain long, aligned lamellae that alternate between ice crystals and ceramic walls.[6,11,12] Subsequent sublimation of the ice yields a green ceramic preform with porosity in a nearly exact replica of the ice crystals. Partial sintering of the green ceramic results in a structure with two distinct and independently controlled levels of porosity[13]: macroporosity, left by the sublimation of solvent crystals (typically 2–200 μm) and microporosity, which is composed of interparticle porosity left by partial sintering (typically <1 μm). The faster a sample is frozen, the finer its macroporosity will be. At the same time, increasing the sintering temperature will result in a decrease of microporosity. It is important to understand the link between processing conditions and microstructure because by controlling the freezing and sintering conditions separately, porous ceramics with a wide range of microstructures can be obtained.[6]

The microstructure of a freeze-cast is defined by its wavelength (λ), which is the average thickness of a single ceramic wall plus its adjacent macropore.[11] Several publications have reported the effects of solidification kinetics on the microstructures of freeze-cast materials.[6,11,12,14–17] It has been shown that λ follows an empirical power-law relationship with solidification velocity v ($\lambda \propto v^{-n}$).[12] However, nearly all of the studied systems have been for single-material dispersions such as alumina or zirconia. Research on the freeze-casting of composites is scarce, specifically with regards to electrochemical ceramics. The few research groups that have used freeze-casting for SOFC applications have focused solely on the anode.[1,5,18,19] The goal of this study is to develop the ability to controllably synthesize freeze-cast ceramics for SOFC cathodes using the parameters of freezing rate, slurry viscosity, and solid loading. The effects of these variables on solidification velocity and λ will be explored. For this work, we will be using the established SOFC composite cathode combination of lanthanum strontium manganite (LSM) for electronic conduction and yttria-stabilized zirconia (YSZ) for ionic conduction.[4,8,20] In addition, the compositional homogeneity of the composite ceramic will be studied to confirm its potential as a cathode material.

II. Experimental Procedure

(1) Slurry Preparation

Five different slurries were used in this study, three to test the effect of the amount of dispersant (1.6, 2.0, and 2.4 wt%

of the solids) with 23 vol% solids and two others to test the effect of solid loading (17 and 27 vol%) using an intermediate viscosity (2.0 wt% dispersant) slurry. The levels of dispersant used, though relatively high, were found to be necessary to maintain particle dispersion and slurry workability. All slurries were prepared at pH = 7.5 as numerous studies have reported the leaching of Yttria ions from YSZ powders in acidic environments[21] and additionally, high pH (≥9) slurries resulted in colloidal destabilization. All slurries were prepared by mixing deionized water with a small amount (1.6, 2.0, and 2.4 wt% of the powder) of an ammonium polymethacrylate dispersant (Darvan C-N; R.T. Vanderbilt Co., Norwalk, CT) at neutral pH. The solution was stirred for 20 min to ensure complete dissolution of the dispersant. The pH of the solution was adjusted back to neutral using nitric acid and then YSZ powder (d_{50} = 0.3 μm, TZ-8Y; Tosoh, Grove City, OH) was slowly added. The colloid was sonicated (S-450A; Branson Ultrasonics, Danbury, CT) while mixing to ensure good dispersion. The pH was again readjusted back to neutral with nitric acid and LSM powder (d_{50} = 0.8 μm, LSM20-P; NexTech Materials, Lewis Center, OH) was slowly added under continued sonication. After the LSM powder had been completely dispersed, 1 wt% (of the solids) of polyethylene glycol binder (Union Carbide Inc., Danbury, CT) was incorporated into the slurry. The ratio of LSM to YSZ was kept at a constant 40:60 vol%, respectively, as this has been shown to be an effective ratio for achieving optimal electrical performance for SOFC cathodes.[22,23]

(2) Rheological Testing
The rheological properties of the various slurries were evaluated using a Haake VT550 Rotational Viscometer (Thermo Fisher Scientific, Inc., Waltham, MA) with an SV-2P type sensor and concentric cylinder (SVP) geometry. The viscosities were measured at ambient temperature using a controlled stepwise shear rate from 20 to 200 s^{-1} to best reveal the non-Newtonian nature of the slurries.

(3) Freeze Casting and Solidification Velocity
Slurries were frozen using a copper cooling rod attached to a liquid nitrogen reservoir. The freezing temperature was monitored and controlled using a PID Controller (CN7800; Omega, Stamford, CT) with a heating sleeve and thermocouple placed around the copper cooling rod near the freezing surface. Dynamic freezing profiles, using linearly decreasing freezing temperatures, were used to promote constant-sized ice lamellae and ceramic walls along the lengths of the freeze-casts.[12,14,17] The decreasing freezing temperature counters the effect of the increasing thermal buffer imposed by the growing ice front, ensuring constant solidification velocity at the freezing front and yielding a highly predictable, anisotropically porous structure.

Before freezing, slurries were placed in a vacuum desiccator to remove any dissolved air. Slurries were then poured into cylindrical acrylic molds approximately 17 mm in diameter and 25 mm tall that had been attached with vacuum grease to the copper cooling finger. Liquid nitrogen was used to linearly decrease the temperature of the copper rod at controlled rates of 1°C/min, 3°C/min, and 5°C/min while the top of the mold remained open to ambient conditions. Cooling from room temperature ensured homogenous and aligned nucleation and growth.[11,24] After complete solidification, the castings were freeze-dried (FreeZone 1L; Labconco, Kansas City, MO) for a minimum of 12 h. The green bodies were carefully removed from their molds and then partially sintered by heating to 450°C at 2°C/min, holding for 30 min and then to 1200°C at 5°C/min with a 2 h dwell time (CM Rapid TEMP Furnace; Bloomfield, NJ). This sintering temperature was chosen as it gives a good compromise between strength and residual porosity. Sintering temperature was

kept constant for all the samples in this study to isolate the effects of freezing rate, viscosity, and solid loading on the microstructure.

An image of the solidification front was taken each minute during freeze-casting using a digital single-lens reflex camera with a macro lense and a timed-automatic shutter release (Fig. 1). By measuring the solidification position as a function of time, the instantaneous solidification velocity at any point in time was estimated. Using this information we were able to correlate the experimental variables of freezing rate, amount of dispersant, and solid loading with freezing velocity and the resultant microstructure.

(4) Processing Parameter Matrix
As described in Sections II(1) and (3), the effect of controllable processing variables on the resultant microstructure was evaluated. The controlled parameters and their levels are summarized in Table I.

(5) Microstructural Characterization
Total, open, and closed porosities of the produced freeze-cast composites were derived from their apparent densities which were measured using Archimedes Method. Replicates from each experimental treatment were then infiltrated with a low-viscosity resin (Buehler GmbH; EpoHeat, Irvine, CA) to provide strength during sectioning and polishing, and contrast for the imaging process. Samples were cross-sectioned at 2 mm intervals along the freezing direction, polished, and imaged with a high-resolution optical microscope (BX-51; Olympus-America Inc., Central Valley, PA) at 20x magnification. Macropore and ceramic wall sizes were each measured separately (~30 measurements each per cross-section resulting in a total of over 500 measurements for samples subjected to the same treatment) to determine their individual dependen-
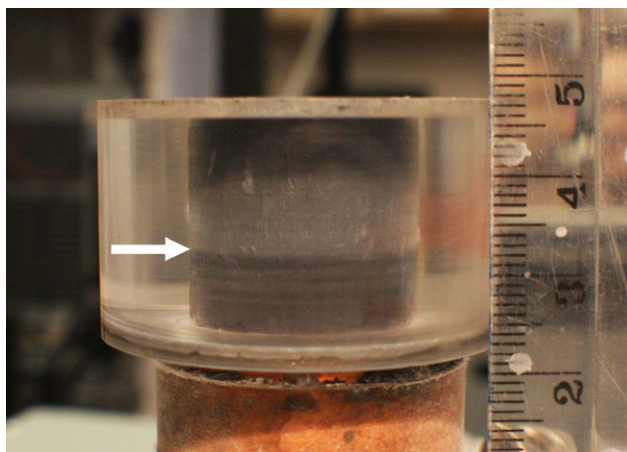

Fig. 1. Solidification of a 23 wt% solids slurry freezing at 5°C/min. This image was taken 10 min. into the solidification process. The darker region below the arrow on the lower third of the sample is the frozen slurry.

Table I. Experimental Parameters

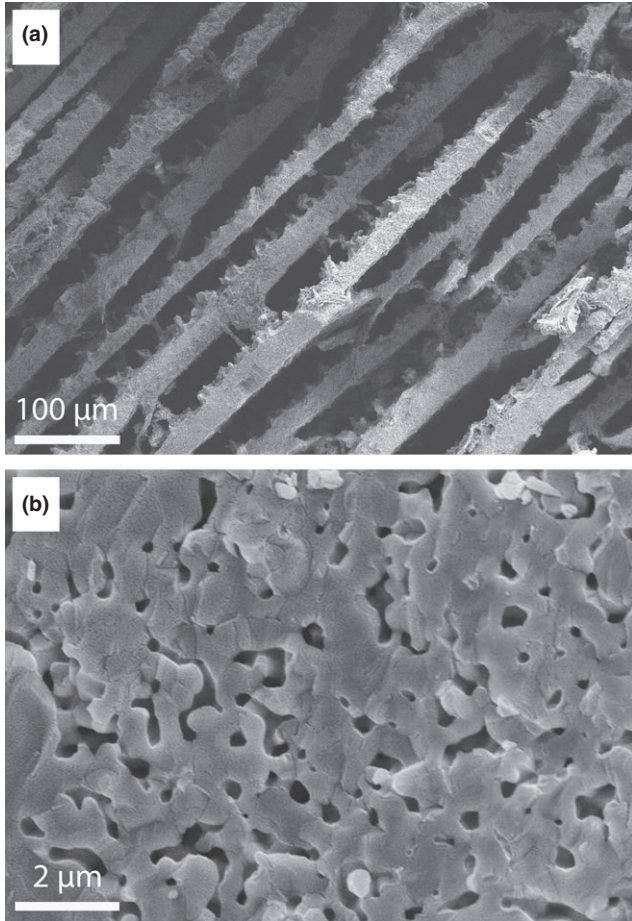|		Solid loading (vol%)	Amount of dispersant (wt%)	Freezing rate (°C/min)
I	Effect of freezing rate	23	2.0	1, 3, 5
II	Effect of slurry viscosity	23	1.6, 2.0, 2.4	5
III	Effect of solid loading	17, 23, 27	2.0	5

Fig. 2. (a) Scanning electron microscope image of LSM-YSZ macroporosity created by ice lamellae. Freezing direction is normal to the page and (b) magnified image of a freeze cast wall showing microporosity left by partial sintering. Sample is 23 vol% solids, contains 2.0 wt% dispersant and was frozen at 5°C/min.
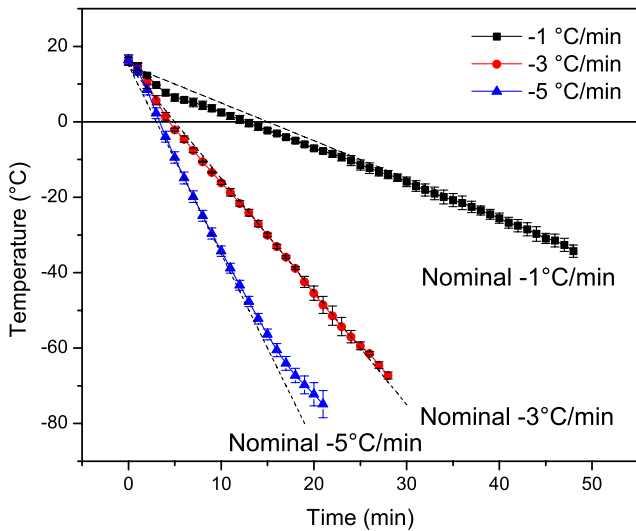

Fig. 3. Plot of experimental and nominal temperatures profiles for the copper freezing finger versus time for the 1°C/min, 3°C/min, and 5°C/min freezing rates. Error bars represent three to seven measurements.

cies on freezing rate, dispersant, and solid loading. The measurements of wall and macropore size from each cross-section were averaged and then added together to determine the overall average λ.

(6) Elemental Mapping

To confirm the dispersion of both LSM and YSZ powders in the porous composites, elemental mapping was performed on representative samples from each experimental treatment. Mapping was done using a scanning electron microscope (SEM, JSM-7000F; JEOL-USA, Inc., Peabody, MA) coupled with electron dispersive X-ray spectroscopy.

III. Results

The produced LSM-YSZ freeze-cast composites were robust and displayed two distinct levels of porosity (Fig. 2): macropores that result from the sublimation of the aligned ice crystals and microporosity in the walls of the macropores.

(1) Effect of Processing Variables

The different experimental variables of freezing rate, amount of dispersant (viscosity), and solid loading were initially tested to determine if they provided distinguishable and statistically adequate datasets. Experimental and nominal
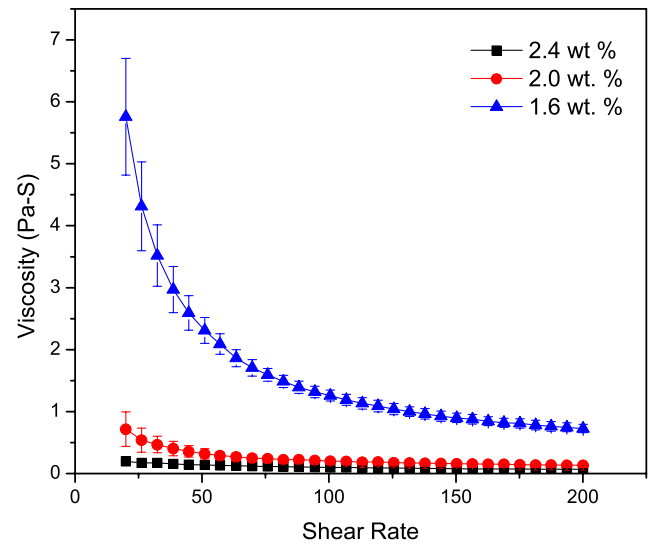

Fig. 4. Viscosity curves for 23 vol% solid slurries with various amounts of dispersant. The curves showed that there was a significant change in viscosity when dispersant levels were changed.
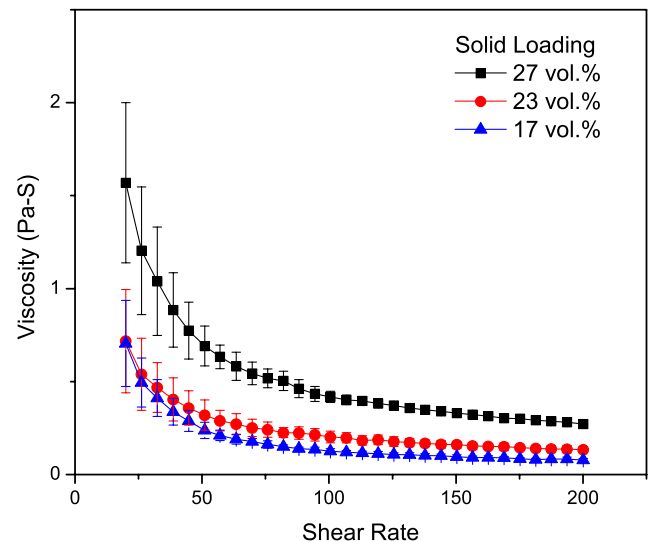

Fig. 5. Viscosity curves for various solid loadings using 2.0 wt% dispersant. Notice that the effect of solid loading is less significant than altering the ratio of dispersant to powder (Fig. 4).

temperature profiles for the three different freezing rates are shown in Fig. 3.

Temperature profile data show that the experimental profiles fit the nominal profiles of 1°C/min, 3°C/min, and 5°C/min within ±1.1°C, 0.5°C, and 1.0°C, respectively, indicating that our experimental setup is capable of following a preset profile with accuracy and precision.

All tested slurries exhibited a clear shear-thinning behavior with viscosity decreasing with increasing shear rate. Rheological testing also shows that there is a significant decrease in viscosity when the level of dispersant is increased from 1.6 to 2.4 wt% (Fig. 4).
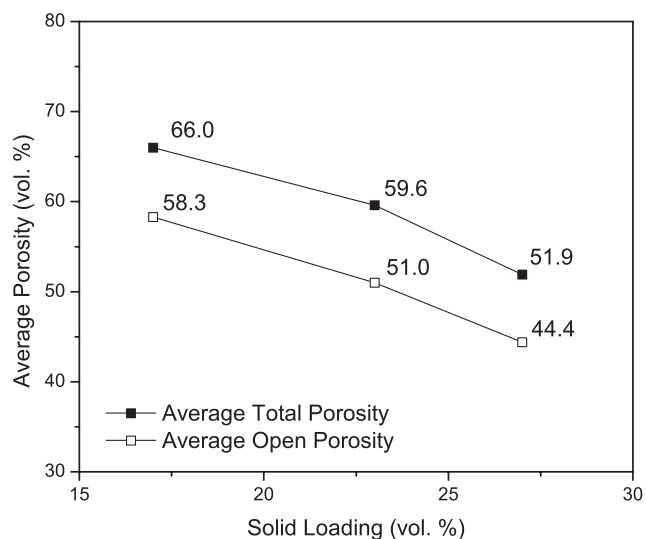
At high shear rates, the 1.6 wt% dispersant slurry was six times more viscous than the 2.0 wt% dispersant slurry and more than ten times as viscous as the 2.4 wt% dispersant slurry. At low shear rates the 1.6 wt% dispersant slurry was eight times more viscous than the 2.0 wt% slurry and more than 29 times as viscous as the 2.4 wt% slurry. Rheological testing was also conducted on the slurries with varying levels of solids (Fig. 5).

It was found that solid loading had a less profound effect on slurry viscosity than the amount of dispersant. At high shear rates the 27 vol% slurry was only 3.5 times more viscous than the least viscous (17 vol%) slurry. As solid loading had little influence on slurry viscosity for this solid loading range we were able to assume that the amount of dispersant and solid loading would act as independent variables and their contributions to the resultant freeze-cast properties would be distinguishable from one another.

It was determined that solid loading was the only variable that had a measurable effect on porosity levels (Fig. 6).

Porosity levels of partially sintered freeze-casts varied approximately linearly with initial solid loading for all samples regardless of freezing rate or viscosity, verifying that the total porosity of LSM-YSZ freeze casts is independent of microstructure and is only a reflection of initial solid loading in the slurry, a conclusion which is supported by a number of other studies using different material systems.[6,7,11,12] The level of closed porosity remains constant at approximately 7.5% ± 0.1% for all samples sintered under the same conditions. This result is consistent with previously reported studies.[25,26]

Fig. 6. Average total porosity and open porosity as a function of initial solid loading. Error bars were not added to the graph because they were smaller than the symbols.

(2) Solidification Velocity and Microstructural Wavelength

The independent effects of freezing rate, dispersant amount, and solid loading were investigated on solidification velocity and λ. The solidification images taken during freeze casting were used to calculate the instantaneous solidification velocities for each sample during the entire freeze-casting
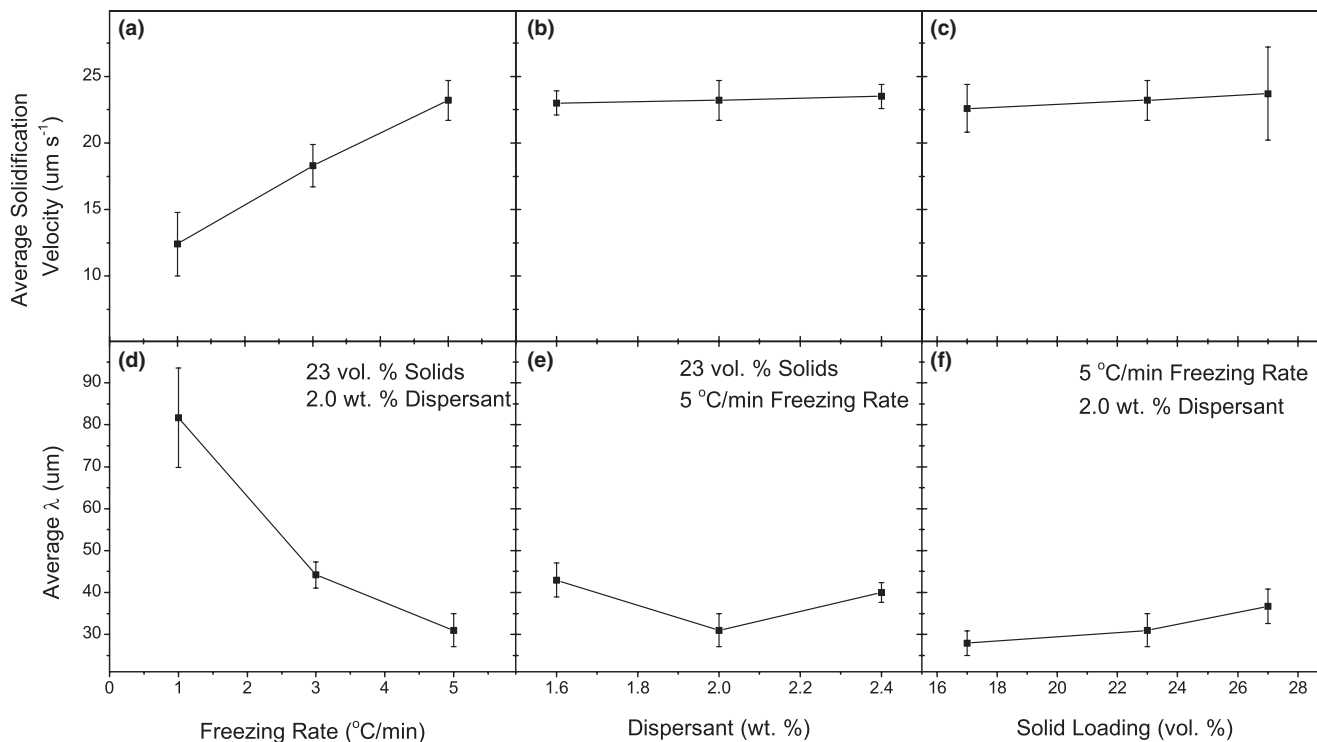

Fig. 7. Plots of average constant solidification velocity as functions of (a) freezing rate; (b) amount of dispersant; and (c) solid loading. Error bars represent the range from a minimum of 18 measurements. Only freezing rate had a significant effect on solidification velocity indicating that viscosity and solid loading have little effect on freezing kinetics. Average λ size as a function of (d) freezing rate; (e) amount of dispersant; and (f) solid loading. Error bars represent the range for a minimum of 500 measurements.

experiment. Using the velocities it was possible to determine the region in which solidification occurs at a constant velocity. Our freeze-casting setup produced samples with nearly constant-sized λ from ~6 to 14 mm along the freezing direction. The freezing velocities measured from the constant solidification regions were averaged and compared across each experimental treatment to see which factors, if any, affected the average solidification velocity of composite LSM-YSZ freeze-casts (Fig. 7). Average λ values as a function of each experimental variable have been plotted directly below the solidification velocity plots to better understand the interrelationships between experimental processing, freezing velocity, and resultant microstructure.

From the freezing velocity plots [Figs. 7(a)–(c)] it was found that the only variable that had a significant effect on the freezing velocity was freezing rate. Increasing the freezing rate from 1°C/min to 5°C/min increased the average solidification velocity from 12 to 23 μm/s which corresponded to a decrease in average λ from 82 to 31 μm [Fig. 7(d)]. Altering solid loading and viscosity had no significant effect on the freezing velocity indicating that solidification velocity is mainly dictated by the thermal profile and the solvent being used.[11]

The effect of the amount of dispersant (slurry viscosity) on λ is complex. It appears that at intermediate levels of dispersant (2.0 wt%) the average microstructural wavelength of a freeze-cast will be approximately 10 ± 2 μm smaller than those of freeze-casts made with either low or high levels of dispersant [Fig. 7(e)]. It is believed that the behavior exhibited by these samples could be attributed to the competing effects of supercooling and particle mobility. Increased levels of dispersant will decrease slurry viscosity (Fig. 5) and enhance the effect of freezing point depression and supercooling of the slurry before it freezes, altering the nucleation regime and subsequent growth[27]; while decreasing dispersant levels (increasing viscosity) hinders ice growth by introducing resistances to particle mobility.[28] It is however unknown what the exact extent of these competing factors is for the LSM-YSZ system. More investigations need to be conducted to determine the effects of viscosity on microstructure.

Interestingly, although solidification velocity did not change with different solid loadings, average λ increased from 28 to 36 μm with an increase in solid loading from 17 to 27 vol% [Fig. 7(f)], with the most noticeable effect occurring at the highest solid loading. It can be assumed from this
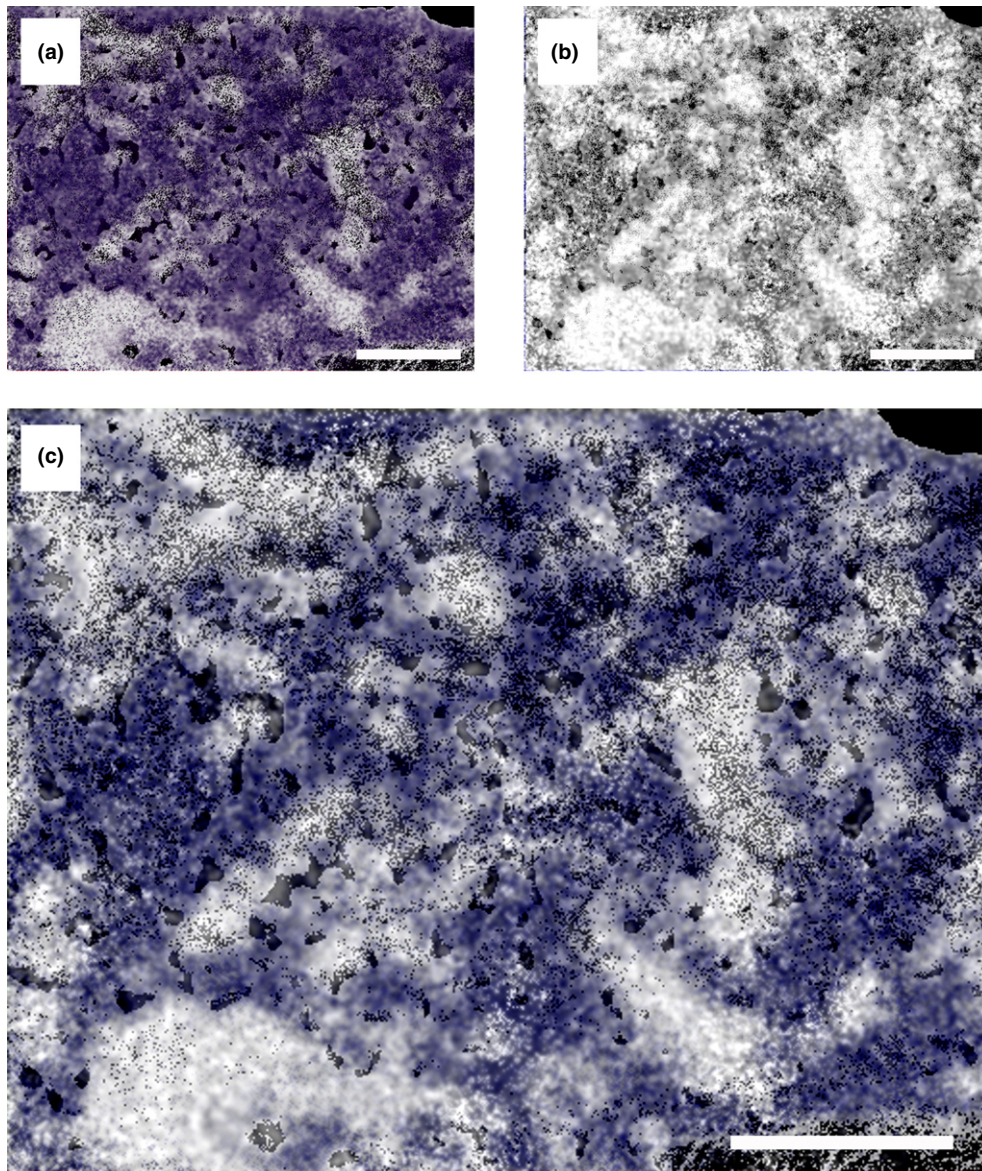

Fig. 8. Elemental map of (a) Zirconia (Blue - Online, Dark Grey - In Print); (b) Lanthanum (White); and (c) the composite elemental distribution within a single wall of a freeze-cast (1.6 wt% dispersant and 23 vol% solids). Freezing direction is normal to the page for all images. Micron bars equal 2 μm.

observation that an increase in wall thickness (from increased solid loading) does not lead to an equivalent decrease in macropore size and vice versa. There is clearly an additional contribution to λ apart from solidification velocity. Both from the effect of dispersant and solid loading, it is clear that λ is not solely determined by the solidification velocity.

(3) LSM-YSZ Dispersion

Elemental mapping revealed that the LSM and YSZ phases are well distributed after processing for each of the five different slurries including those with different levels of dispersant. A representative map is shown in Fig. 8.

There are no excessively large clusters of LSM or YSZ visible in any of the compositional maps although the structure does seem to be characterized by the presence of small agglomerates possibly due to the nonideal dispersion made necessary by the two-particle materials system. The good distribution of the two phases will allow for percolation of electronic and ionic conducting particles throughout the cathode.[8,20] For a fuel cell electrode, however, percolation along the macropores, where gaseous species flow, are especially important. Any deficiencies in LSM along the ceramic wall boundaries would be particularly detrimental to performance. Mapping of an entire wall, from macropore to macropore, showed even distribution of the two phases across the entire ceramic wall (Fig. 9).

IV. Discussion

(1) Aqueous Dispersion of LSM-YSZ

The first challenge to creating anisotropic freeze-casts of LSM and YSZ required a stable aqueous dispersion with an adequate degree of fluidity for freeze-casting.[6] The LSM and YSZ particles that were used have significantly different size distributions, $d_{50} = 0.8$ and 0.3 μm, respectively. The different sizes and densities of the particles lead to differing drag forces for LSM and YSZ. Preliminary tests showed that for slurries with low viscosities the YSZ and LSM would separate from one another. The lighter, smaller YSZ would tend to segregate from the large, heavy LSM, resulting in a non-homogenous distribution of particles. It was found that by increasing the viscosity of the slurry by decreasing the amounts of dispersant, one could create a stable dispersion while still maintaining the workability necessary to make a freeze casting. It is believed that the increased viscosity prevented slurry destabilization by decreasing particle mobility.[29] Solidification velocity testing [Fig. 7(b)] confirms that freezing kinetics were unaffected by the increased viscosity.

The dispersant levels chosen for this experiment were found to be the limits of what the LSM-YSZ slurry could support. At low levels of dispersant (high viscosities), the slurries were so viscous that they were unable to properly settle in their molds, the resultant structures contained many voids, cracks, and defects that rendered them extremely weak. On the other end of the spectrum, high levels of
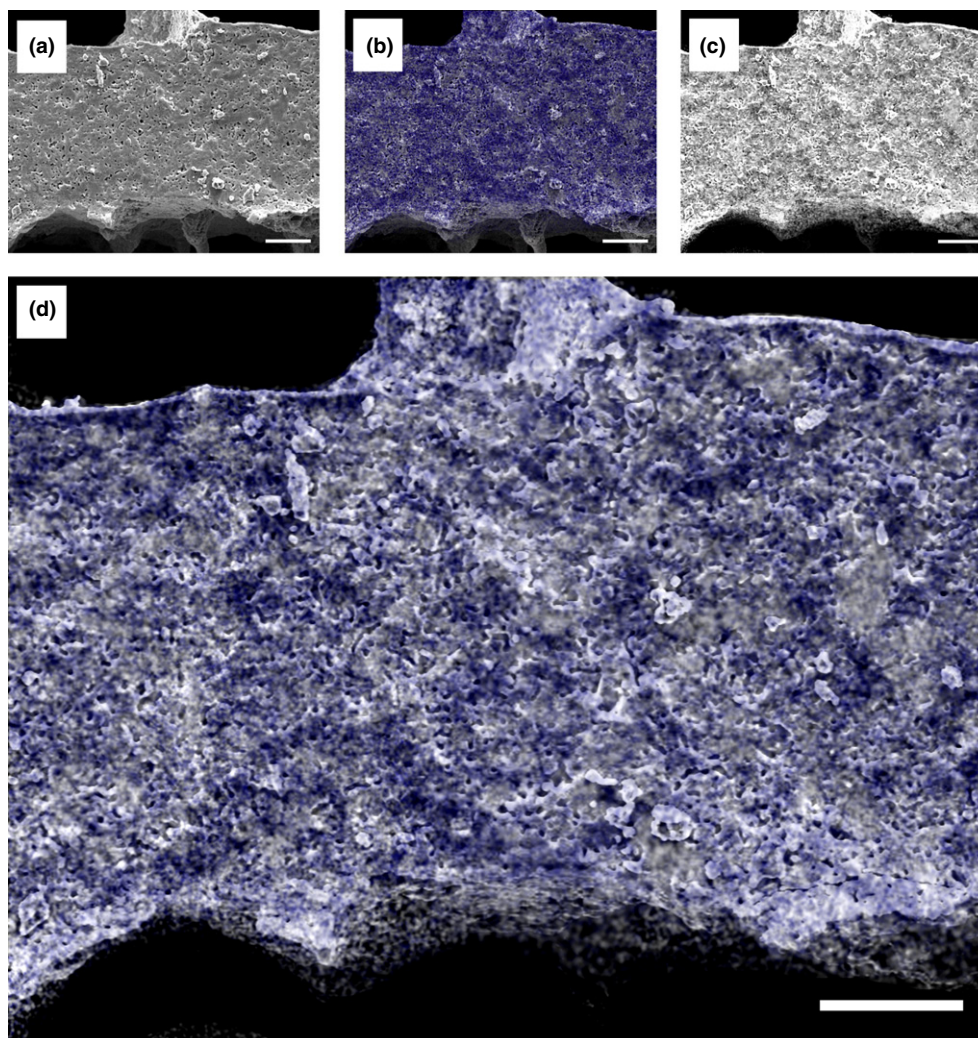

Fig. 9. (a) Scanning electron microscope image of an entire freeze-cast ceramic wall (1.6 wt% dispersant and 23 vol% solids); (b) zirconia map (blue - online, dark grey - in print); (c) lanthanum map (white); and (d) composite elemental distribution from macropore to macropore. Freezing direction is normal to the page for all images. Micron bars equal 10 μm.

dispersant led to slurry destabilization which resulted in a heterogeneous distribution of LSM and YSZ in the final ceramic.

(2)   Microstructural Control

As reported by Deville *et al.*,[6,11] microstructural wavelength is empirically dictated by a power-law:

$$\lambda = Av^{-n} \qquad (1)$$

where *n* represents the effect of solidification velocity (v) on microstructural wavelength (λ) and the prefactor (*A*) represents the contributions from the initial slurry, i.e., solid loading, viscosity, etc. By plotting average λ as a function of solidification velocity on a log scale (Fig. 10), we find that the experimentally derived average λ values for the LSM-YSZ system is also well approximated by this expression where *A* is 4034 and *n* is 1.5. The *n*-value derived from these experiments is larger than those found for alumina ($n = 0.8$–1.3)[11,17] indicating that λ, for LSM-YSZ freeze-casts, shows

a stronger dependence on solidification velocity which is actually advantageous for microstructural tailoring. The *n*-value has been shown to be dependent on particle size[11,27] therefore, our large *n*-value could be partially attributed to the relatively large particle sizes ($d_{50\text{LSM}} = 0.8$ μm, $d_{50\text{YSZ}} = 0.3$ μm) being used. Using Eq. (1), average λ for freezing velocities in the proximity of those investigated here can be predicted, making this a powerful tool for tailored LSM-YSZ microstructures.

When solid loading is altered, both v and the *n*-value remain constant; however, there is still a positive trend for average λ with solid loading [Fig. 7(f)]. Using Eq. (1) with constant v and *n*, an expression for *A* with respect to solid loading was found and plotted in Fig. 11. It was determined that *A* can be approximated as a linear function where *x* is the solid loading fraction (vol%) of the slurry. As both v and *n* remained constant for this experiment, it is the change in *A* as a function of the solid loading that is responsible for the increase in average λ. To identify any specific changes on the microstructural level, the thickness of the ceramic walls and macropores were separated and individually plotted (Fig. 12).

It was found that the rate of ceramic wall growth does not equal the rate of macropore size decrease. For increasing solid contents, average wall size increased more than twice as fast as the decrease in average macropore size. It is this unequal wall-to-pore size change which accounts for the increasing average λ with solid loading [Fig. 7(f)].

Using the empirical relationship from Eq. (1), it can be seen that λ is exponentially dependent, and therefore highly sensitive, to changes in v and only linearly dependent on the *A*-value. For a given set of experimental conditions, there will be an equilibrium solidification speed v^* and an equilibrium ice crystal. The size of this equilibrium crystal is predominantly related to v^*, as the thickness of an ice crystal is directly proportional to the speed at which it freezes.[11] The thickness of the ceramic walls is a function of the space available between the growing ice crystals. Increasing the solid loading (Fig. 12) will result in increased wall size to account for the increased solid fraction, however, because solidification velocity remains unchanged [Fig. 7(c)], the ice crystals will be biased towards remaining their equilibrium size at v^*. It is for this reason that average λ increases [Fig. 7(f)] even though solidification velocity remained consistent [Fig. 7(c)]. This allows for the ratio of wall-to-pore size
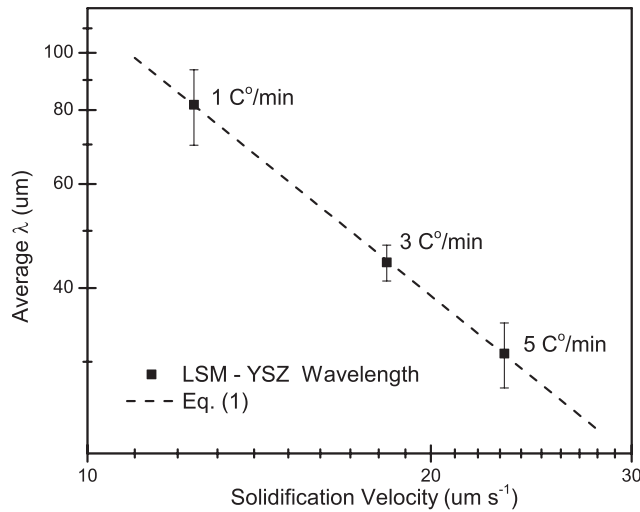

Fig. 10. Average λ as a function of solidification velocity (for the 1°C/min–5°C/min samples). Dispersant and solid loading are held constant at 2.0 wt% and 23 vol%, respectively. The data have been plotted on a log scale and fit with a power law (*R*-value > 0.99) to be used as a predictive relationship.
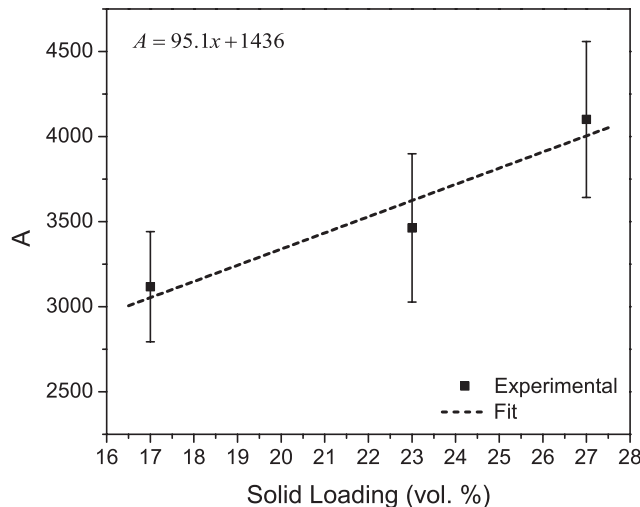

Fig. 11. A as a function of solid loading. All data were taken at a freezing rate of 5°C/min, and the values for v and *n* were 23 μm/s and 1.5, respectively (*R*-value > 0.92).
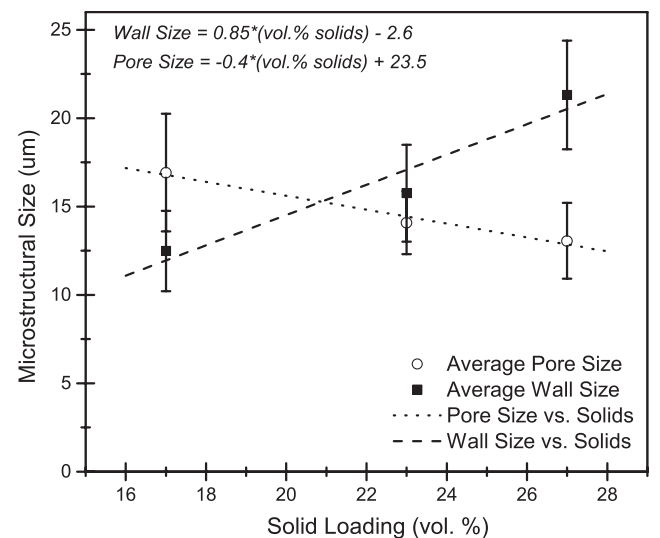

Fig. 12. Plot of average microstructural size as a function of solid loading (vol%). Open circles represent macropores while black squares represent wall sizes. Using a linear trendline it was determined that the wall size (*R*-value > 0.93) increased faster than the macropore size decreased (*R*-value > 0.97).
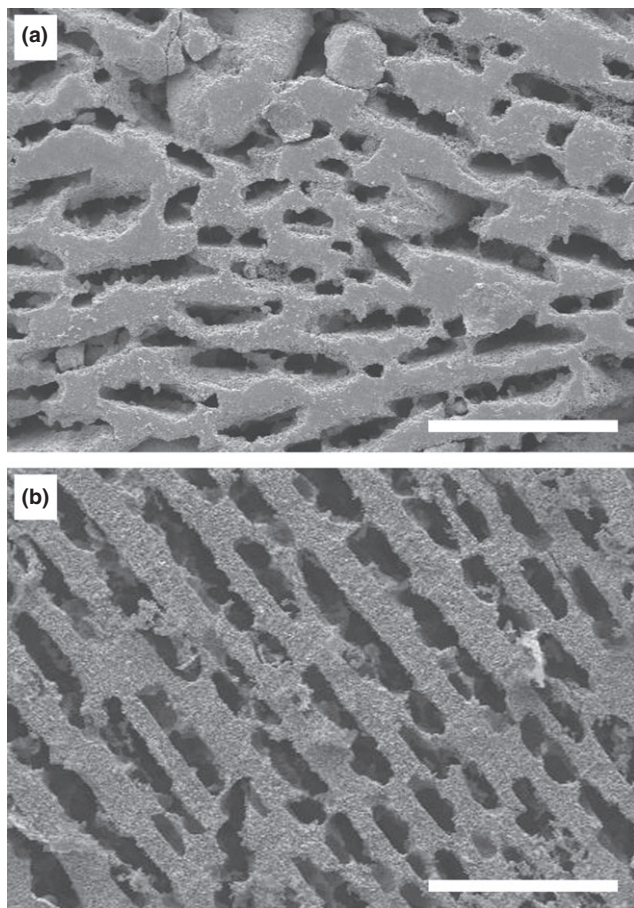
Fig. 13. Images of (a) 27 vol% and (b) 17 vol% freeze-casts frozen at 5°C/min taken from cross-sections at 6 mm along the freezing direction. Walls are light in color and the pores are dark. Notice that the change in the average wall thickness (70% difference) between the two images is significantly larger than the change in pore thickness (26% difference). Micron bar equals 100 μm in each image.

to be tuned while holding pore size approximately constant (Fig. 13).

The suppressed effect of solid loading on macropore size is only the case for a limited range of solid loadings. At high solid loadings (>80 wt%)[11] particle–particle interactions begin to have a significant impact on the impinging freezing front,[28,30] additionally, particle redistribution during solidification becomes difficult and the ice crystals will engulf the ceramic particles rather than pushing them aside. The result is an isotropic, dense structure.

V. Conclusions

Anisotropic, hierarchically porous microstructures with uniaxially aligned pores for SOFC cathodes were controllably fabricated by directionally freeze casting aqueous dispersions of LSM and YSZ powders. The resultant composites show good dispersion of the electronic and ionic conducting particles, they are robust and display excellent control of porosity (52–66 ± 0.34 vol%), and average λ (31–82 ± 6.3 μm). Average λ can be precisely controlled by controlling the freezing rate and is well approximated by a simple power-law providing a method for the design and prediction of microstructures. In addition, the ratio of wall-to-pore size can be tuned using the solid loading.

Freezing rate was found to be the only significant factor affecting freezing velocity indicating that the freezing process is primarily a function of the freezing kinetics of the solvent and the thermal conditions of the system. Total and open porosity were found to be independent of microstructure and only affected by the initial solid loading of the slurry. Viscosity was found to have no significant effect on freezing velocity and only a minor although complex effect on microstructural characteristics, although its effect on dispersion of particles and creating workable slurries was critical.

The prefactor, *A*, in Eq. (1) is proportional to the microstructural wavelength, λ. The *A*-value was found to linearly depend on the solid loading. An additional effect of solid loading was on the total porosity. Finally, the micro-porosity appears to depend on the sintering conditions. Thus, this investigation has shown that it is possible to independently control the microstructural wavelength, total porosity, and the relative amount of micro- and macro-porosity.

References

[1]S. W. Sofie, "Fabrication of Functionally Graded and Aligned Porosity in Thin Ceramic Substrates with the Novel Freeze-Tape-Casting Process," *J. Am. Ceram. Soc.*, **90**, 2024–31 (2007).
[2]K. Wincewicz and J. Cooper, "Taxonomies of SOFC Material and Manufacturing Alternatives," *J. Power Sources*, **140**, 280–96 (2005).
[3]J. Molenda, K. Świerczek, and W. Zając, "Functional Materials for the IT-SOFC," *J. Power Sources*, **173**, 657–70 (2007).
[4]A. T. Duong and D. R. Mumm, "Microstructural Optimization by Tailoring Particle Sizes for LSM–YSZ Solid Oxide Fuel Cell Composite Cathodes," *J. Electrochem. Soc.*, **159**, B40–53 (2012).
[5]J. Moon, H. Hwang, M. Awano, and K. Maeda, "Preparation of NiO–YSZ Tubular Support with Radially Aligned Pore Channels," *Mater. Lett.*, **57**, 1428–34 (2003).
[6]S. Deville, "Freeze-Casting of Porous Ceramics: A Review of Current Achievements and Issues," *Adv. Eng. Mater.*, **10**, 155–69 (2008).
[7]C. Tallon and G. V. Franks, "Recent Trends in Shape Forming from Colloidal Processing: A Review," *J. Ceram. Soc. Jpn.*, **119**, 147–60 (2011).
[8]B. Kenney and K. Karan, "Engineering of Microstructure and Design of a Planar Porous Composite SOFC Cathode: A Numerical Analysis," *Solid State Ionics*, **178**, 297–306 (2007).
[9]E. S. Greene, W. K. S. Chiu, and M. G. Medeiros, "Mass Transfer in Graded Microstructure Solid Oxide Fuel Cell Electrodes," *J. Power Sources*, **161**, 225–31 (2006).
[10]F. Tietz, A. Mai, and D. Stöver, "From Powder Properties to Fuel Cell Performance –A Holistic Approach for SOFC Cathode Development," *Solid State Ionics*, **179**, 1509–15 (2008).
[11]S. Deville, E. Saiz, and A. P. Tomsia, "Ice-Templated Porous Alumina Structures," *Acta Mater.*, **55**, 1965–74 (2007).
[12]T. Waschkies, R. Oberacker, and M. J. Hoffmann, "Control of Lamellae Spacing During Freeze Casting of Ceramics Using Double-Side Cooling as a Novel Processing Route," *J. Am. Ceram. Soc.*, **92**, S79–84 (2009).
[13]S. Deville, E. Saiz, and A. P. Tomsia, "Freeze Casting of Hydroxyapatite Scaffolds for Bone Tissue Engineering," *Biomaterials*, **27**, 5480–9 (2006).
[14]A. Preiss, B. Su, S. Collins, and D. Simpson, "Tailored Graded Pore Structure in Zirconia Toughened Alumina Ceramics Using Double-Side Cooling Freeze Casting," *J. Eur. Ceram. Soc.*, **32**, 1575–83 (2012).
[15]S. S. L. Peppin, J. A. W. Elliott, and M. G. Worster, "Solidification of Colloidal Suspensions," *J. Fluid Mech.*, **554**, 147 (2006).
[16]L. Hu, C.-A. Wang, Y. Huang, C. Sun, S. Lu, and Z. Hu, "Control of Pore Channel Size during Freeze Casting of Porous YSZ Ceramics with Unidirectionally Aligned Channels Using Different Freezing Temperatures," *J. Eur. Ceram. Soc.*, **30**, 3389–96 (2010).
[17]T. Waschkies, R. Oberacker, and M. J. Hoffmann, "Investigation of Structure Formation During Freeze-Casting From Very Slow to Very Fast Solidification Velocities," *Acta Mater.*, **59**, 5135–45 (2011).
[18]Y.-H. Koh, J.-J. Sun, and H.-E. Kim, "Freeze Casting of Porous Ni–YSZ Cermets," *Mater. Lett.*, **61**, 1283–7 (2007).
[19]Y. Chen, J. Bunch, T. Li, Z. Mao, and F. Chen, "Novel Functionally Graded Acicular Electrode for Solid Oxide Cells Fabricated by the Freeze-Tape-Casting Process," *J. Power Sources*, **213**, 93–9 (2012).
[20]M. J. L. Ostergard, C. Clausen, C. Bagger, and M. Mogensen, "Manganite–Zirconia Composite Cathodes for SOFC: Influence of Structure and Composition," *Electrochim. Acta*, **40**, 1971–81 (1995).
[21]F. Snijkers, A. de Wilde, S. Nullens, and J. Luyten, "Aqueous Tape Casting of Yttria Stabilised Zirconia Using Natural Product Binder," *J. Eur. Ceram. Soc.*, **2** [24] 1107–11 (2004).
[22]L. C. R. Schneider, C. L. Martin, Y. Bultel, D. Bouvard, and E. Seibert, "Discrete Modelling of the Electrochemical Performance of SOFC Electrodes," *Electrochim. Acta*, **52**, 314–24 (2006).

[23]A. Abbaspour, J. Luo, and K. Nandakumar, "Electrochimica Acta Three-Dimensional Random Resistor-Network Model for Solid Oxide Fuel Cell Composite Electrodes," *Electrochim. Acta*, **55**, 3944–50 (2010).

[24]H. Schoof, J. Apel, I. Heschel, and G. Rau, "Control of Pore Structure and Size in Freeze-Dried Collagen Sponges," *J. Biomed. Mater. Res.*, **58**, 352–7 (2001).

[25]N. Shanti, K. Araki, and J. Halloran, "Particle Redistribution during Dendritic Solidification of Particle Suspensions," *J. Am. Ceram. Soc.*, **89**, 2444–7 (2006).

[26]S. Deville and G. Bernard-Granger, "Influence of Surface Tension, Osmotic Pressure, and Pores Morphology on the Densification of Ice-Templated Ceramics," *J. Eur. Ceram. Soc.*, **31**, 983–7 (2011).

[27]S. Deville, E. Maire, A. Lasalle, A. Bogner, C. Gauthier, J. Leloup, and C. Guizard, "Influence of Particle Size on Ice Nucleation and Growth during the Ice-Templating Process," *J. Am. Ceram. Soc.*, **93**, 2507–10 (2010).

[28]S. S. L. Peppin, M. G. Worster, and J. S. Wettlaufer, "Morphological Instability in Freezing Colloidal Suspensions," *Proc. R. Soc. Lond. A*, **463**, 723–33 (2007).

[29]S. Deville, E. Maire, G. Bernard-Granger, A. Lasalle, A. Bogner, C. Gauthier, J. Leloup, and C. Guizard, "Metastable and Unstable Cellular Solidification of Colloidal Suspensions," *Nat. Mater.*, **8**, 966–72 (2009).

[30]A. Lasalle, C. Guizard, E. Maire, and S. Deville, "Particles Redistribution and Structural Defects Development during Ice Templating," *Acta Mater.*, **60**, 4594–603 (2012). □